ACS Photonics

ACS Editors' Choice

Article

pubs.acs.org/journal/apchd5

Terms of Use

Ultranarrow Luminescence Linewidth of Silicon Nanocrystals and Influence of Matrix

Ilya Sychugov,*[,†] Anna Fucikova,[†] Federico Pevere,[†] Zhenyu Yang,[‡] Jonathan G. C. Veinot,[‡] and Jan Linnros[†]

[†]Material and Nano Physics Department, ICT School, KTH−Royal Institute of Technology, 16440 Kista, Sweden

[‡]Department of Chemistry, University of Alberta, Edmonton, Alberta T6G 2G2, Canada

Supporting Information

ABSTRACT: The luminescence linewidth of individual silicon nanocrystals was characterized by single-dot spectroscopy, and an ultranarrow linewidth of ∼200 μeV at 10 K was found. This value is, in fact, limited by system resolution and represents only the upper limit of the homogeneous linewidth. In addition, the effect of the matrix was investigated for nanocrystals coated with organic ligands, embedded in silicon dioxide, as well as for nanocrystals with only a thin passivating layer. It was found that, depending on the matrix, the room-temperature bandwidth may vary by an order of magnitude, where values as small as ∼12 meV (∼5 nm) at 300 K were detected for nanocrystals with a thin passivation. The observed values for silicon nanocrystals are similar and even surpass some of those for direct-band-gap quantum dots. The narrow linewidth at room temperature enables the use of silicon nanocrystals for nontoxic narrow-band labeling of biomolecules and for application as phosphors in white-light-emitting devices.

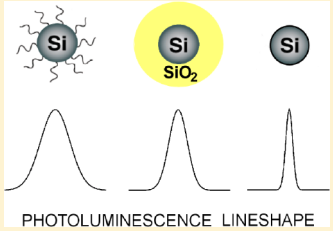

KEYWORDS: *silicon nanocrystals, photoluminescence, surface passivation, linewidth*

The discovery of strong, visible luminescence from porous silicon two decades ago[1] brought hope for applications in optoelectronics such as a long-sought silicon-based light source for on-chip optical communication. Although the demonstrated quantum efficiency was relatively high, the microsecond-long luminescence lifetime indicated the indirect-band-gap nature of the optical transition remained, limiting high-speed and high-brightness applications. The nanostructured network of the porous silicon (p-Si) and the tunable emission wavelength pointed toward a quantum confinement mechanism of the light emission, although other surface-related mechanisms were proposed.[2] Later, similar luminescence was demonstrated in different systems involving silicon nanocrystals (NCs) embedded in oxide, e.g., prepared by ion implantation[3] or co-deposition[4] with subsequent annealing.

The wide emission spectrum of porous silicon (typically 150−200 nm) was also a serious limitation for potential applications and was generally believed to stem from a wide size distribution (so-called inhomogeneous linewidth) in the p-Si skeleton.[2] Thus, activities toward narrowing the size distribution were initiated by, for example, size selection of porous silicon particles.[5] This resulted in some narrowing; however the emission spectrum essentially remained wide (Figure 1, blue curve). Finally, single-dot spectroscopy studies of individual Si nanocrystals, performed by this[6] and other groups,[7] also yielded broad homogeneous linewidths of ∼100−200 meV (∼40−80 nm at ∼700 nm wavelength) at room temperature, significantly broader than those exhibited by direct-band-gap quantum dots. Line-narrowing at reduced temperatures was, however, demonstrated later, reaching ∼2 meV at 35 K.[8] Again, it is only marginally smaller than the thermal broadening and is still much larger than the natural limit set by the uncertainty principle (see Discussion). At the same time, theoretical calculations predicted broad spectra could originate from phonon-mediated radiative recombination.[9] In any case, what sets the linewidth in an indirect-band-gap material nanocrystal remained unclear, and one may ask whether it is sample

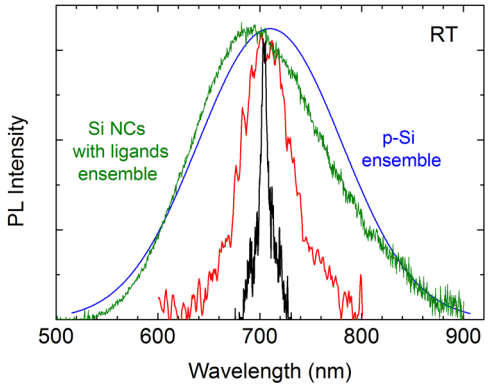

Figure 1. Room-temperature luminescence spectra from an ensemble of size-selected porous silicon particles (blue, ref 5) and of ligand-passivated silicon nanocrystals (green, this work), from a single silicon nanocrystal in a SiO_2 shell (red, ref 6), and with only a thin passivating layer (black, this work). The effect of matrix on the homogeneous linewidth (black to red) can be as significant as inhomogeneous broadening (red to blue, green), increasing the linewidth several times.

Received: June 19, 2014
Published: September 11, 2014

dependent and what the roles of the interface and matrix would be.

In the past decade different protocols for chemical synthesis of colloidal silicon nanoparticles have been proposed. Typically these methods include fabrication of a nanocrystal-rich solid-state matrix with subsequent release of nanoparticles into a solution. Among them are thermal processing of hydrogen silsesquioxane (HSQ),[10] silane combustion,[11] hydrofluoric acid treatment of magnetron-sputtered films,[12] silane decomposition in nonthermal plasma,[13] or laser pyrolysis.[14] Direct synthetic methods, such as laser ablation in liquid[15] and microwave-assisted reaction,[16] have also been investigated. A significant advantage of the colloidal form of Si quantum dots is the possibility of surface chemistry modification. In general, along with the size of nanocrystals, surface passivation is recognized as an important parameter affecting optical properties. It was shown, for instance, that passivation of Si NCs with organic ligands instead of silicon oxide can improve quantum yield and shift their luminescence spectrum.[17] The surface engineering of nanoparticles in a solution is not only limited to chemical reactions but can also be extended to, for example, microwave or plasma treatment.[18] These recent developments made possible mass fabrication of Si NCs, which can be tailored for different applications as passive fluorophores.

One such application is luminescent labeling, where quantum dots have clear advantages for *in vitro* and *in vivo* imaging when compared with conventional fluorescent dye molecules.[19] Among the benefits are reduced sensitivity to microenvironments due to capping of the quantum dot core, better photostability under strong excitation, and spectral multiplexing (i.e., possibility for parallel detection where a wide absorption spectrum enables the use of a single pump source). The biocompatibility and biodegradability of silicon[20] becomes an important factor in this field, considering that many standard solutions of prototypical quantum dots include toxic elements such as cadmium. It was indeed shown that silicon nanocrystals can be used for cell imaging,[21,22] single-molecule tracking,[23] and *in vivo* studies.[24]

Another area where quantum dots find an application niche is solid-state lighting. Today white-light-emitting diodes (LEDs) are often composed of a blue-emitting GaN diode and rare-earth elements, which act as phosphors for partial down-conversion of the light frequency, resulting in a broadband emission of the device.[25] In order to avoid the use of scarce rare-earth elements, different methods are being investigated, such as Mn doping of glass.[26] Nanocrystals offer an alternative route considering their relatively high luminescent quantum yields that approach those of rare-earth elements.[25] It has been reported that the luminescent quantum yield of silicon nanocrystals can reach up to 60%,[27,28] making them attractive nontoxic material candidates.

For any of the above-mentioned applications one of the most important parameters is the luminescence linewidth. Indeed, it has been shown that the spectral purity of quantum dots can substantially improve the color rendering index and the correlated color temperature of an LED.[25] Parallel detection in biolabeling also requires size-separated quantum dots to be free from overlapping emission spectra.[19] In general, the linewidth of a quantum dot ensemble is a convolution of the homogeneous Γ_{hom} and inhomogeneous Γ_{inh} broadening:

$$\Gamma = \sqrt{\Gamma_{hom}^{2} + \Gamma_{inh}^{2}}$$

For CdSe nanocrystals the typical room-temperature values are $\Gamma \approx 20-35$ nm[25] and $\Gamma_{hom} \approx 15-20$ nm.[29] As discussed above, in previous measurements of oxidized Si nanocrystals Γ_{hom} was found to be 3−4 times larger than for CdSe nanoparticles. These values imply that even perfect size-selection would not provide a narrow ensemble linewidth for this material, where the individual luminescence linewidth appears to be a limiting factor.

In this paper, we report the narrowest linewidths ever observed, to our knowledge, for Si nanostructures both at low and at room temperature. We demonstrate a significant narrowing of the spectrum for free-standing silicon nanocrystals with a thin passivation layer (Figure 1, narrowest peak) compared to oxide- and ligand-embedded nanoparticles. In contrast to previous studies the effect of spectral diffusion was minimized here by virtue of a more sensitive instrument allowing for shorter acquisition times. It is also found that reduced shell thickness for the same matrix leads to narrower linewidth, explaining previous observations of broad low-temperature as well as room-temperature lines for nanoparticles in a thicker oxide. Thus, on the basis of single-dot spectroscopy of differently passivated nanocrystals we clarify the effect of the surrounding matrix on the nanocrystal emission bandwidth and provide an explanation in the context of exciton scattering with specific acoustic phonon modes. It is shown that detected luminescence linewidth values for indirect-band-gap material quantum dots in fact do not differ from that of direct-band-gap nanoparticles, revealing similarities of these two types of semiconductor materials at the nanoscale.

EXPERIMENTAL AND RESULTS

Three different sample preparation procedures were used to form silicon nanocrystals in target matrices: (i) Silicon dioxide capped nanocrystals were fabricated in an ultrathin layer of a low-doped silicon-on-insulator wafer by thermal oxidation. In this case, crystalline nanostructures of different sizes can form randomly due to the unevenness (on a few nanometer level) of the top silicon layer. The oxidation time was very short (less than a minute at 900 °C), leading to the formation of a thin (i.e., only a few nanometers) oxide shell around the nanocrystals.[30]

Second, (ii) ligand-functionalized silicon nanocrystals were produced using a well-established chemical synthesis,[10] where it was shown recently that oligomer chains are typically formed on the surface.[31] An HSQ solution (Fox-17, 74 wt % solution in methyl isobutyl ketone) from Dow Corning was dried under vacuum to remove the solvent. The resulting white powder was thermally processed at 1100 °C (ramp up temperature 18 °C min^{-1}) in a 5% H_2/95% Ar atmosphere for an hour. The resulting amber solid was ground to a fine brown composite powder consisting of Si NCs in a SiO_2 matrix. Hydride-terminated Si NCs were liberated from the Si NC/SiO_2 composite using HF etching[32] and extracted from the etching solution using toluene. Surface functionalization of Si NCs with dodecyl was achieved via thermal or radical (azobis-(isobutyronitrile) at 60 °C) initiation, and the solution was stirred at 60 °C for 15 h until a transparent orange solution was obtained. The dodecyl-functionalized particles were purified by repeated solvent/antisolvent (toluene/ethanol) precipitation, centrifugation, decantation, and redispersion in toluene. Following three cycles, the Si NC stock solution was filtered through a 0.45 μm polytetrafluoroethylene syringe filter. An ensemble photoluminescence spectrum of such nanocrystals in

dx.doi.org/10.1021/ph500221z | ACS Photonics 2014, 1, 998−1005

solution is shown in Figure 1 (green) and appears to be similar to porous silicon particle emission. For single-particle optical characterization the stock solution was diluted 100× upon addition of dry toluene and spin-coated (6000 rpm for 30 s) on a piece of cleaned silicon wafer.

Finally, (iii) to prepare silicon nanocrystals without a definite matrix, a similar protocol as in (ii) was used except for nanoparticle extraction and surface functionalization steps. A commercial HSQ resist from Dow Corning (type XR-1541, 10 wt % solution in methyl isobutyl ketone) was spin-coated on a piece of cleaned silicon wafer and left to dry for 24 h. Then it was annealed at 1000 °C in 5% H_2 and 95% Ar for an hour. The resulting film had a porous structure and was about 100 nm thick as seen in cross-sectional transmission electron microscope images.[33] It contained silicon nanocrystals with Si−O−R^I bonds on the surface, as revealed by TEM, Fourier-transform infrared measurements, and optical characterization.[33] Unlike in the previous case, no additional deliberate measures were taken to affect the nanocrystal surface for this sample. We will refer to such nanocrystals as passivated only or thin-shell particles, implying the lack of continuous elastic media around them, since their thin shell is partly or largely exposed to air when embedded in a porous film.

The presence of crystalline Si nanoparticles was confirmed in all samples by TEM, and they were comprehensively characterized using standard methods as described elsewhere.[10,30−33] On the basis of ensemble lifetime and single-dot excitation power-dependent measurements (not shown) we have found that exciton lifetime in all these nanoparticles is in the microsecond range, typical for Si NCs. Here their temperature-dependent optical response was evaluated using a microphotoluminescence apparatus with single-particle detection capability. The instrument is equipped with a liquid flow cryostat (Oxford Instruments) that can operate with liquid nitrogen or helium, where the sample is held on the coldfinger under vacuum for thermal insulation from the cryostat glass. A blue laser diode (405 nm) was applied in continuous wave mode for dark-field, nonresonant excitation. An imaging spectrometer (Andor Shamrock 500) with two different gratings of spectral resolution, 0.9 and 0.08 nm (∼200 μeV in the nanocrystal emission range), and a thermoelectrically cooled, intensified charge-coupled device camera (Andor iXon-3) were used for signal detection. This optical system has an order of magnitude better spectral resolution and higher sensitivity than the one used in previous studies.[8] A key procedure toward recording ultranarrow luminescence spectra at low temperature was a sequential recording of 10−100 spectra at a relatively short time scale (∼2 min each) in order to reveal "spectral diffusion". The detected linewidth naturally broadens if such random displacement of the emission peak occurs, and this effect can be reduced by selecting relatively stable dots or by using a short acquisition time (see video in the Supporting Information). For comparison we note that with the previous optical system[8] the acquisition time was ∼30 min to get a good signal-to-noise ratio.

A representative room-temperature spectrum from a "passivated only" nanoparticle is shown in Figure 1 (black line). It is seen that for the same emission wavelength the linewidth is clearly narrower than from nanoparticles embedded in SiO_2 (red line). With decreasing temperature the linewidth decreases for all three types of silicon nanoparticles. In Figure 2 an example of a low-temperature spectrum from an oxide-embedded nanocrystal is presented. The spectrum is nearly

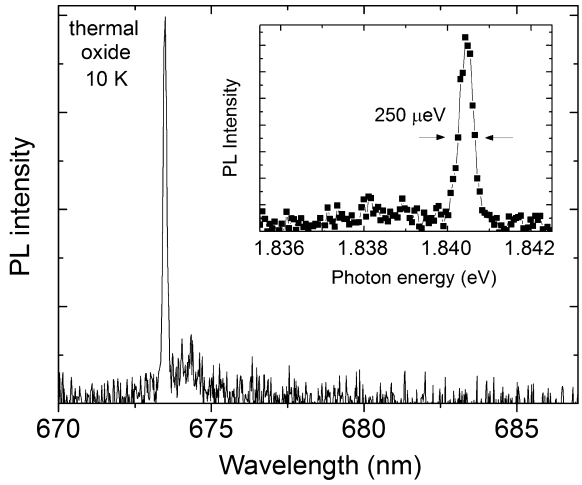

Figure 2. Low-temperature narrow luminescence spectrum of an individual Si nanocrystal, embedded in silicon dioxide with a resolved ∼2 meV replica. The linewidth value for the main peak was deconvoluted with a system resolution.

system resolution limited, and we indeed detected a few spectra with a ∼200 μeV linewidth set by the apparatus for thin passivation and oxide-embedded nanocrystals. The high spectral resolution of the optical system used here not only allowed the detection of the ultranarrow luminescence linewidth at low temperature but also facilitated the observation of a clearly resolved ∼2 meV replica in oxide-embedded nanocrystals. The amplitude of this replica appeared to be much smaller than that of the main peak in all cases, while the replica linewidth varied from dot-to-dot. With increasing temperature this replica broadens and eventually merges with the main line. Hence we conclude that this peak is not related to singlet−triplet exciton ground level splitting since in that case the replica would decrease in intensity with increasing temperature, reflecting a reduced population of the lower lying triplet state. Also the value of the singlet−triplet splitting for oxide-embedded nanocrystals emitting in this energy range was measured to be ∼10−15 meV,[2,34] several times larger than the ∼2 meV separation of the replica from the main line detected here. Therefore, following the Boltzmann distribution, at 10 K only the lower lying triplet state can be populated (for 10 meV singlet−triplet splitting energy the relative population of the higher lying singlet state at 10 K should be $\sim 10^{-5}$) and no lower energy peak should be observed. Thus, we attribute this peak instead to nanocrystal-specific acoustic phonon modes, where only the first-order mode of the manifold appears to be above the instrument detection limit. The energy of these modes depends on the matrix and strongly affects the room-temperature bandwidth, as discussed below.

In this work, luminescence properties of individual nanocrystals were analyzed using a statistical approach. In doing so, more than 1000 individual spectra were recorded altogether at different temperatures. An example of the emission peak position distribution is shown in Figure 3 for all three particle types investigated here. The presented spectra were acquired at 70 K. The variation in individual peak position from 1.6 to 2.1 eV can be ascribed to the size-dependent quantum confinement effect in silicon, and the histograms nicely compare to the ensemble spectra of porous silicon[2] or silicon nanocrystals in oxide.[3] Furthermore, a similar emission range for the three particle types indicates a comparable size distribution of

dx.doi.org/10.1021/ph500221z | ACS Photonics 2014, 1, 998−1005

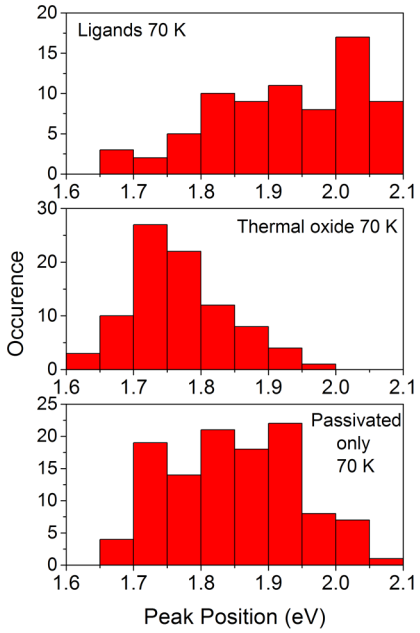

Figure 3. Distribution of emission peak positions for individual silicon nanocrystals with ligands (top), embedded in thermal oxide (middle), and for passivated-only particles (bottom) measured at 70 K.

nanocrystals in these samples. The distribution of ligand-passivated nanoparticles is somewhat broader and slightly shifted to the green spectral region.

While the peak position distributions are similar, the luminescence linewidth of individual particles for these three samples varies significantly. This is demonstrated by the histograms in Figure 4, where we have chosen spectra at 70 K in order not to be limited by the system resolution. Ligand-modified silicon nanocrystals exhibit broad emission lines, while the luminescence from oxide-encapsulated particles is narrower

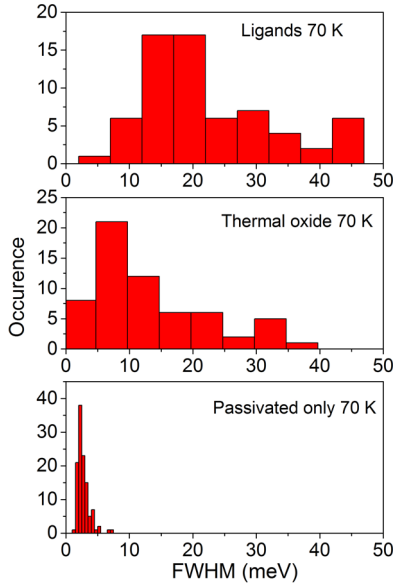

Figure 4. Statistical distributions of the spectral linewidth (full width at half-maximum) for individual nanocrystals at 70 K for particles with ligands (top), oxide-encapsulated nanocrystals (middle), and passivated-only nanoparticles (bottom). Bin width is 5 meV in the top two charts but reduced to 0.5 meV in the last chart for clarity.

and passivated-only nanocrystals emit in extremely narrow bands. Below, we outline a reasonable explanation for the origin of the matrix-dependent linewidth broadening by invoking an exciton−phonon scattering effect.

DISCUSSION

In general, the ultimate limit of a linewidth for a given energy state is defined by the uncertainty principle:

$$\Delta E \approx \frac{\hbar}{\Delta t} \tag{1}$$

For direct-band-gap semiconductor nanocrystals the lifetime is on the order of nanoseconds,[29] corresponding to the natural limit of ∼0.1 μeV. Experimentally, linewidth values close to the ultimate limit were deduced from the accumulated photon echo measurements for CuCl (∼1 μeV),[35] InGaAs (∼2 μeV),[36] and CdSe (∼1.6 μeV)[37] quantum dots.

On the other hand, silicon quantum dots exhibit a microsecond lifetime that is 3 orders of magnitude larger than in their direct-band-gap counterparts.[38] The origin of this important difference is an indirect band gap of the corresponding bulk material, where such zero-phonon transitions are forbidden due to the *k*-conservation rule. At the nanoscale this selection rule is partly relaxed as a result of the quantum confinement effect.[39,40] Together with possible exciton localization, this leads to the observed zero-phonon emission line with a weak oscillator strength.[30] The ultimate limit on the linewidth of such a transition would then be ∼0.1 neV. In practice, however, a solid-state system with such a long lifetime would inevitably suffer from different perturbations such as exciton−phonon interactions or external fluctuating charges. The random charges manifest in spectral diffusion or hopping of the emission line, which was, for instance, observed in thermally oxidized nanocrystals and occurs at long time scales, such as seconds or even minutes[41] (see Supporting Information for a video of spectral diffusion). On the other hand, exciton−phonon scattering is a fast process resulting in broadening of the emission linewidth; this is discussed in detail below.

In nanocrystals, along with bulk-related vibrational modes, there is a specific class of phonon modes that can be described by Lamb's theory of elastic body vibrations for small particles.[42] These modes can be spherical or torsional, depending on whether the vibration takes place with or without radial displacement. Experimentally the modes can be measured on particle ensembles using Raman scattering[43] or for single particles using luminescence spectroscopy (cf. Figure 2). However, it was found that Lamb's theory, describing the behavior of free-standing particles alone, does not adequately explain experimental data obtained from oxide-passivated silicon nanocrystals.[43] The influence of the surrounding matrix on vibrational mode energy was proposed, and later, indeed, calculations for different core/shell configurations yielded different phonon modes.[44] In fact, the elasticity of the matrix plays an important role in defining the frequency of such "breathing" vibrations. It is believed that unlike optical phonon modes, which manifest in the sidebands of the luminescence spectrum, such low-energy acoustic phonons cause energy fluctuations of the exciton level, resulting in homogeneous broadening of the emission linewidth.[45] Then the temperature dependence of the linewidth should reflect Bose−Einstein statistics of the thermal population for these phonon modes.[8]

dx.doi.org/10.1021/ph500221z | ACS Photonics 2014, 1, 998−1005

Here we consider individual silicon nanocrystals emitting in a similar spectral range (cf. Figure 3), indicating their similar size distribution, but embedded in different matrices. Their acoustic mode energies can be estimated from

$$\varepsilon_{S,T}^{\ln} = \hbar\omega_{S,T}^{\ln} = \hbar\chi_{S,T}^{\ln}\frac{C_{L,t}}{R} \tag{2}$$

where l and n are angular momentum and principle quantum numbers, S and T are spherical and torsional modes, $C_{L,t}$ is the longitudinal and transverse speed of sound, R is nanoparticle radius, and χ is a calculated value.[44]

To identify the most relevant mode for the present case (n and l values), first we note that silicon is a nonpolar semiconductor, where piezoelectric electron−phonon coupling does not exist. So the selection rules derived for a zincblende crystal, such as CdSe, are not applicable.[45] The coupling here is caused by deformation potential only, and we apply selection rules as described in ref 46. In the luminescence experiment phonon creation is associated with the light emission process. Since the photon emission is electric dipolar, it will create a phonon of the dipolar spheroidal mode only (l = 1), and not spherical (l = 0) or quadruple (l = 2) modes. It was independently demonstrated that the contribution from torsional modes to exciton−phonon interaction in Si nanocrystals is 2−3 orders of magnitude smaller than from spheroidal modes.[45] Then, by limiting consideration to the lowest order mode only (n = 0), the phonon energy values become for ligand-functionalized particles $\varepsilon_S^{10}(\mathrm{lig}) \approx 0.7$ meV, for the Si/SiO_2 system $\varepsilon_S^{10}(\mathrm{ox}) \approx 2.5$ meV, and for passivated only particles $\varepsilon_S^{10}(\mathrm{po}) \approx 10$ meV. The longitudinal speed of sound averaged over crystallographic directions, 4 nm particle diameter, and calculated χ^{10} values for three different matrices[44] were used. The presence of a few meV modes in the luminescence spectrum of SiO_2-embedded nanocrystals was indeed observed here from oxidized nanolayers (cf. Figure 2) as well as previously from oxidized nanopillars[8] and nanowalls.[47]

The energy of the mode, in turn, defines exciton−phonon coupling strength.[45] For a given mode the coupling strength is inversely proportional to the square of the mode energy:

$$S = \left(\frac{\gamma}{\varepsilon}\right)^2 \tag{3}$$

where the proportionality coefficient γ is a matrix element (coupling constant) of the electron−phonon interaction Hamiltonian. Thus, the lower energy modes present in ligand-passivated nanocrystals are much more strongly coupled to the exciton than the same modes, but with a higher energy, inherent to passivated-only particles. The weaker coupling strength explains the lack of consistent observation of phonon replicas in the latter case, where the emission line shape is usually found to consist of a main line only. On the other hand, very small phonon mode energy in the case of a ligand layer makes it indistinguishable from the main emission line in photoluminescence experiments.

Finally, the mode energy also defines the temperature evolution of the emission linewidth. The number of phonons in an energy state ε as a function of temperature k_BT is defined by Bose−Einstein statistics:

$$n \sim \frac{1}{\exp(\varepsilon/k_BT) - 1} \approx (k_BT >> \varepsilon) \approx \frac{k_BT}{\varepsilon} \tag{4}$$

From eq 4 one can see that at the high-temperature limit the number of phonons is linearly proportional to temperature, where the proportionality coefficient is the inverse mode energy. In Figure 5, we have plotted average fwhm values

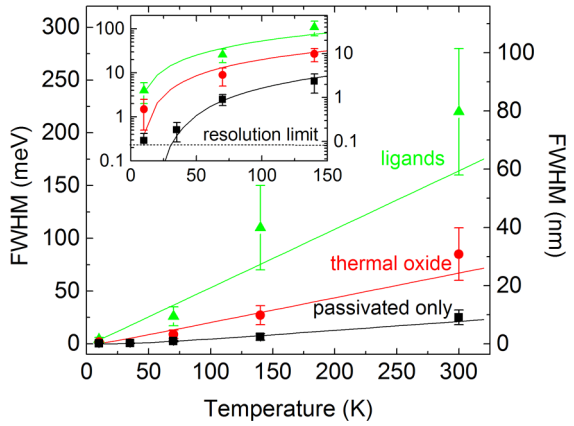

Figure 5. Temperature evolution of the average value of the luminescence linewidth for individual Si nanocrystals with ligands (triangles), in dioxide (circles), and for passivated-only particles (squares). Error bars show the width of the fwhm statistical distribution. The solid line is a fit based on phonon population statistics for 0.7, 2.5, and 10 meV intrinsic acoustic modes, correspondingly. Measured linewidth values in meV were for reference recalculated to nm for 1.85 eV emission photon energy (right axis). Inset shows low-temperature data in log-scale for clarity.

measured at various temperatures for individual Si nanocrystals with a thin shell only, in the oxide, and in ligand matrices. The fit to the data points is based on phonon population statistics (eq 4) for three intrinsic energy modes (0.7, 2.5, and 10 meV), where the scaling coefficient is the only fitting parameter for all these configurations. One can see that the temperature evolution of the emission linewidth can be described well by invoking specific vibrational modes whose energy strongly depends on the surrounding matrix. It is in fact impossible to fit, for example, the data for nanocrystals with ligand passivation using phonon mode energies of thin-shell nanocrystals and vice versa. At higher temperatures, as expected from Bose statistics, the linewidth grows linearly, where the slope is inversely proportional to the phonon energy, leading to a narrower linewidth for thin passivation particles. As a result, the average room-temperature bandwidth can vary by an order of magnitude: from ∼25 meV for passivated-only particles to ∼220 meV for dodecene-functionalized particles, depending on the encapsulating layer elastic properties. Error bars in Figure 5 reflect variations from dot-to-dot in, for example, size, for the same type of surface passivation since the acoustic mode energy has strong size-dependence.[45] In addition, single-nanocrystal shape may deviate from an ideal sphere, resulting in splitting of the lowest order breathing mode into several direction-dependent modes. These modes may have slightly different energies, leading to the observation of broad replica peaks instead of well-defined sharp replica lines in individual spectra (cf. Figure 2), and may also contribute to the observed dot-to-dot linewidth variations. However, we believe that the strongest effect on the homogeneous linewidth comes from the matrix elastic properties, where the specific phonon energy may vary by more than an order of magnitude, as estimated above.

dx.doi.org/10.1021/ph500221z | ACS Photonics 2014, 1, 998−1005

The above-mentioned estimations for oxide- and ligand-embedded particles are based upon the infinite matrix assumption. For real nanocrystals, however, the finite thickness of the surrounding layer could also affect the vibrational mode energy and, hence, the room-temperature linewidth. In Figure 6, we compare linewidth distributions for individual nanocrystals embedded in SiO_2 of different thickness. Nanocrystals obtained from time-limited (i.e., 10 s at 900 °C) or native oxide-only nanolayers were compared with those formed by long self-limiting oxidation of nanopillars (i.e., 1 h at 900 °C). From TEM images the oxide thickness is 15−20 nm for the latter and 3−5 nm for the former case (inset in Figure 6). Indeed the distribution of the emission linewidth is shifted to smaller values for the thinner oxide thickness, where nanocrystals approach elastic stress-free nanoparticle configuration. We note here that initial measurements on oxidized nanocrystals[6,8] were performed on particles with a thick oxide shell, leading to the observation of broad emission lines. So it is possible to obtain narrow luminescence linewidths with a careful design of the preparative method for a given material/matrix target. Recently, the same dependence of the linewidth on the shell thickness was observed in CdSe/CdS core/shell nanocrystals.[48]

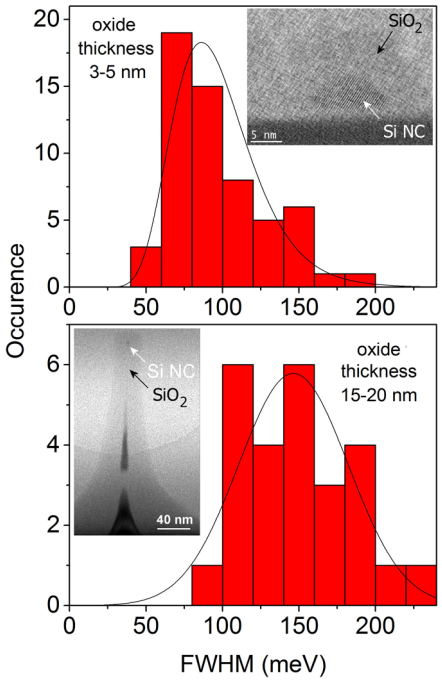

Figure 6. Statistical distribution of the spectral linewidth for individual nanocrystals in a SiO_2 matrix at room temperature (top) for nanolayer samples with a thin oxide passivation layer and (bottom) for nanopillar samples with a thick oxide layer. Solid lines are guides for the eye. Typical TEM images are shown in the insets.

To put these results in perspective, we compare a typical luminescence linewidth of silicon nanocrystals measured by single-dot spectroscopy in this work with literature values for direct-band-gap nanocrystals characterized by the same technique. While time-domain measurements can give higher resolution at low temperature,[35−37] photoluminescence measurements are more important practically since they directly correspond to the situation where nanocrystals can be applied as phosphors or biolabels. Temperature evolution of the emission linewidth can also be studied, providing insight into the observed values at room temperature. The data for nanocrystals of different materials are summarized in Table 1

Table 1. Narrowest Low-Temperature Homogeneous Linewidth Deduced from Single-Dot Spectroscopy for Nanocrystals of Different Materials (μeV)

CdSe[49]	CdS[50]	InAs[51]	InP[52]	GaAs[53]	GaN[54]	Si [this work]
<120	~1000	<30	<40	<30	~6000	<200

Table 2. Typical Value of the Room-Temperature Homogeneous Linewidth Deduced from Single-Dot Spectroscopy for Nanocrystals of Different Materials (meV)

CdSe/ZnSe[29]	InAs/GaAs[55]	PbS/polymer[56]	Si/thin shell [this work]	Si/SiO_2 [this work]	Si/ligands [this work]
>50	~20	~100	~25	~90	~220

for the low-temperature and in Table 2 for the room-temperature measurements. It is immediately evident that single-dot spectroscopy at low temperature gives values that are much higher than the ultimate linewidth limit (set by the uncertainty relation) for all quantum dots. The measured values are limited either by the spectral resolution of the detection system or the influences of spectral diffusion, which are especially pronounced in CdS and GaN nanocrystals.[50,54] Thus, the values in Table 1 simply represent upper limits of the linewidth achievable by this method. Taking into account the experimental limitations, one can reasonably expect that silicon quantum dots behave very similarly to their direct-band-gap counterparts regarding the bandwidth absolute value and its temperature evolution. In some cases, such as the room-temperature linewidth for thin-shell nanocrystals, they even outperform CdSe nanocrystals (cf. Table 2), which have been long considered as a model system for optical studies of quantum dots.

CONCLUSIONS

In this paper we report the observation of ultranarrow emission lines from single silicon nanocrystals/quantum dots at low temperature. The observed linewidth, ~200 μeV at 10 K, can in fact be much lower since this value is the limit of our system resolution. Comparison with linewidths reported for other quantum dot systems and the tunability of the emission for various dots strongly support a quantum-confined mechanism for the luminescence from silicon quantum dots. We have also demonstrated that the mechanical coupling of a nanocrystal to its matrix largely influences the luminescence linewidth due to exciton−phonon interaction. This can be minimized using a thin passivating layer, resulting in a relatively sharp linewidth even at room temperature (as narrow as ~5 nm). These results unequivocally show that previous theoretical models predicting necessary broadening due to the indirect band-gap structure of silicon were incorrect, having general implications for modeling and applications of silicon nanostructures. In fact, only now when the homogeneous linewidth has been reduced, methods to address a smaller size distribution to reduce the inhomogeneous broadening can be applied. Mass fabrication of narrow-linewidth individual nanocrystals reported here and their size-separation by centrifuging or charge-separation by

dx.doi.org/10.1021/ph500221z | ACS Photonics 2014, 1, 998−1005

high-performance chromatography would be the next experimental steps to achieve narrow-linewidth ensembles.

Thus, a direct application of understanding the phonon contributions to the photoluminescence broadening described in the present study can facilitate the development and application of nanomaterials with narrow spectral linewidths. This can possibly be used for biolabeling and for replacing phosphors in solid-state light-emitting diodes, where silicon nanocrystals have a clear advantage, being a nontoxic and environmentally friendly material.

■ ASSOCIATED CONTENT

Supporting Information

A video file composed of a sequence of spectral images showing the spectral diffusion effect in individual silicon nanocrystals with a description text file. This material is available free of charge via the Internet at http://pubs.acs.org.

■ AUTHOR INFORMATION

Corresponding Author

*E-mail: ilyas@kth.se.

Notes

The authors declare no competing financial interest.

■ ACKNOWLEDGMENTS

Financial support from the Swedish Research Council (VR) through an individual contract and through a Linnaeus grant (ADOPT) is gratefully acknowledged. A.F. thanks the Carl Tryggers Foundation for the postdoc scholarship. Z.Y. and J.V. acknowledge continued generous funding from the Natural Sciences and Engineering Research Council of Canada (NSERC) and University of Alberta Department of Chemistry.

■ REFERENCES

(1) Cullis, A. G.; Canham, L. T. Visible Light Emission Due to Quantum Size Effects in Highly Porous Crystalline Silicon. *Nature* **1991**, *353*, 335−338.

(2) Cullis, A. G.; Canham, L. T.; Calcott, P. D. J. The Structural and Luminescent Properties of Porous Silicon. *J. Appl. Phys.* **1997**, *82*, 909−965.

(3) Guha, S.; Pace, M. D.; Dunn, D. N.; Singer, I. L. Visible Light Emission from Si Nanocrystals Grown by Ion Implantation and Subsequent Annealing. *Appl. Phys. Lett.* **1997**, *70*, 1207−1209.

(4) Daldosso, N.; Das, G.; Larcheri, S.; Mariotto, G.; Dalba, G.; Pavesi, L.; Irrera, A.; Priolo, F.; Iacona, F.; Rocca, F. Silicon Nanocrystal Formation in Annealed Silicon-Rich Oxide Films Prepared by Plasma Enhanced Chemical Vapor Deposition. *J. Appl. Phys.* **2007**, *101*, 113510.

(5) Wilson, W. L.; Szajowski, P. F.; Brus, L. E. Quantum Confinement in Size-Selected, Surface Oxidized Silicon Nanocrystals. *Science* **1993**, *262*, 1242−1244.

(6) Valenta, J.; Juhasz, R.; Linnros, J. Photoluminescence Spectroscopy of Single Silicon Quantum Dots. *Appl. Phys. Lett.* **2002**, *80*, 1070−1072.

(7) Mason, M. D.; Credo, G. M.; Weston, K. D.; Buratto, S. K. Luminescence of Individual Porous Si Chromophores. *Phys. Rev. Lett.* **1998**, *80*, 5405−5408.

(8) Sychugov, I.; Juhasz, R.; Valenta, J.; Linnros, J. Narrow Luminescence Linewidth of a Silicon Quantum Dot. *Phys. Rev. Lett.* **2005**, *94*, 087405.

(9) Delerue, C.; Allan, G.; Lannoo, M. Electron-Phonon Coupling and Optical Transitions for Indirect-Gap Semiconductor Nanocrystals. *Phys. Rev. B* **2001**, *64*, 193402.

(10) Hessel, C.; Henderson, E.; Veinot, J. Hydrogen Silsesquioxane: A Molecular Precursor for Nanocrystalline Si-SiO_2 Composites and Freestanding Hydride-Surface-Terminated Silicon Nanoparticles. *Chem. Mater.* **2006**, *18*, 6139−6146.

(11) Fojtik, A.; Henglein, A. Surface Chemistry of Luminescent Colloidal Silicon Nanoparticles. *J. Phys. Chem. B* **2006**, *110*, 1994−1998.

(12) Sugimoto, H.; Fujii, M.; Imakita, K.; Hayashi, S.; Akamatsu, K. All-Inorganic Near-Infrared Luminescent Colloidal Silicon Nanocrystals: High Dispersibility in Polar Liquid by Phosphorus and Boron Codoping. *J. Phys. Chem. C* **2012**, *116*, 17969−17974.

(13) Mangolini, L.; Thimsen, E.; Kortshagen, U. High-yield Plasma Synthesis of Luminescent Silicon Nanocrystals. *Nano Lett.* **2005**, *5*, 655−659.

(14) Li, X.; He, Y.; Swihart, M. Surface Functionalization of Silicon Nanoparticles Produced by Laser-Driven Pyrolysis of Silane Followed by HF-HNO_3 Etching. *Langmuir* **2004**, *20*, 4720−4727.

(15) Shirahata, N.; Linford, M. R.; Furumi, S.; Pei, L.; Sakka, Y.; Gates, R. J.; Asplund, M. C. Laser-derived One-Pot Synthesis of Silicon Nanocrystals Terminated with Organic Monolayers. *Chem. Commun.* **2009**, 4684−4686.

(16) Atkins, T. M.; Louie, A. Y.; Kauzlarich, S. M. An Efficient Microwave-Assisted Synthesis Method for the Production of Water Soluble Amine-Terminated Si Nanoparticles. *Nanotechnology* **2012**, *23*, 294006.

(17) Kusova, K.; Cibulka, O.; Dohnalova, K.; Pelant, I.; Valenta, J.; Fucikova, A.; Zidek, K.; Lang, J.; Englich, J.; Matejka, P.; Stepanek, P.; Bakardjieva, S. Brightly Luminescent Organically Capped Silicon Nanocrystals Fabricated at Room Temperature and Atmospheric Pressure. *ACS Nano* **2010**, *4*, 4495−4504.

(18) Mariotti, D.; Mitra, S.; Svrcek, V. Surface-Engineered Silicon Nanocrystals. *Nanoscale* **2013**, *5*, 1385−1398.

(19) Resch-Gender, U.; Grabolle, M.; Cavaliere-Jaricot, S.; Nitschke, R.; Nann, T. Quantum Dots versus Organic Dyes as Fluorescent Labels. *Nat. Methods* **2008**, *5*, 763−775.

(20) Low, S. P.; Voelcker, N. H.; Canham, L. T.; Williams, K. A. The Biocompatibility of Porous Silicon in Tissues of the Eye. *Biomaterials* **2009**, *30*, 2873−2880.

(21) Erogbogbo, F.; Yong, K.-T.; Roy, I.; Xu, G.; Prasad, P.; Swihart, M. Biocompatible Luminescent Silicon Quantum Dots for Imaging of Cancer Cells. *ACS Nano* **2008**, *2*, 873−878.

(22) Shiohara, A.; Prabakar, S.; Faramus, A.; Hsu, C.-Y.; Lai, P.-S.; Northcote, P. T.; Tilley, R. D. Sized Controlled Synthesis, Purification, and Cell Studies with Silicon Quantum Dots. *Nanoscale* **2011**, *3*, 3364−3370.

(23) Nishimura, H.; Ritchie, K.; Kasai, R. S.; Goto, M.; Morone, N.; Sugimura, H.; Tanaka, K.; Sase, I.; Yoshimura, A.; Nakano, Y.; Fujiwara, T. K.; Kusumi, A. Biocompatible Fluorescent Silicon Nanocrystals for Single-Molecule Tracking and Fluorescence Imaging. *J. Cell Biol.* **2013**, *202*, 967−983.

(24) Park, J.-H.; Gu, L.; von Matlzahn, G.; Ruoslahti, E.; Bhatia, S. N.; Sailor, M. J. Biodegradable Luminescent Porous Silicon Nanoparticles for in Vivo Applications. *Nat. Mater.* **2009**, *8*, 331−336.

(25) Talapin, D. V.; Steckel, J. Quantum Dot Light-Emitting Devices. *MRS Bull.* **2013**, *38*, 685−691.

(26) Masai, H.; Fujiwara, T.; Matsumoto, S.; Takahashi, Y.; Iwasaki, K.; Tokuda, Y.; Yoko, T. White Light Emission of Mn-Doped SnO-ZnO-P_2O_5 Glass Containing No Rare Earth Cation. *Opt. Lett.* **2011**, *36*, 2868−2870.

(27) Jurbergs, D.; Rogojina, E.; Mangolini, L.; Kortshagen, U. Silicon Nanocrystals with Ensemble Quantum Yields Exceeding 60%. *Appl. Phys. Lett.* **2006**, *88*, 233116.

(28) Miller, J. B.; Van Sickle, A. R.; Anthony, R. J.; Kroll, D. M.; Kortshagen, U. R.; Hobbie, E. K. Ensemble Brightening and Enhanced Quantum Yield in Size-Purified Silicon Nanocrystals. *ACS Nano* **2012**, *6*, 7389−7396.

(29) Schlegel, G.; Bohenberger, J.; Potapova, I.; Mews, A. Fluorescence Decay Time of Single Semiconductor Nanocrystals. *Phys. Rev. Lett.* **2002**, *88*, 137401.

(30) Sychugov, I.; Valenta, J.; Mitsuishi, K.; Fujii, M.; Linnros, J. Photoluminescence Measurements of Zero-Phonon Optical Transitions in Silicon Nanocrystals. *Phys. Rev. B* **2011**, *84*, 125326.
(31) Yang, Z.; Iqbal, M.; Dobbie, A.; Veinot, J. Surface-Induced Alkene Oligomerization: Does Thermal Hydrosilylation Really Lead to Monolayer Protected Silicon Nanocrystals? *J. Am. Chem. Soc.* **2013**, *135*, 17595−17601.
(32) Rodriguez Núñez, J. R.; Kelly, J. A.; Henderson, E. J.; Veinot, J. Wavelength Controlled Etching of Silicon Nanocrystals. *Chem. Mater.* **2012**, *24*, 346−352.
(33) Fucikova, A.; Sychugov, I.; Yang, Z.; Veinot, J.; Linnros, J. One-Step Synthesis of Silicon Nanocrystals with a Thin Shell Embedded in a Porous Organosilicon Film. Manuscript in preparation.
(34) Brongersma, M.; Kik, P.; Polman, A.; Min, K.; Atwater, H. Size-Dependent Electron-Hole Exchange Interaction in Si Nanocrystals. *Appl. Phys. Lett.* **2000**, *76*, 351−353.
(35) Ikezawa, M.; Masumoto, Y. Ultranarrow Homogeneous Broadening of Confined Excitons in Quantum Dots: Effect of the Surrounding Matrix. *Phys. Rev. B* **2000**, *61*, 12662−12665.
(36) Borri, P.; Langbein, W.; Schneider, S.; Woggon, U.; Sellin, R. L.; Ouyang, D.; Bimberg, D. Ultralong Dephasing Time in InGaAs Quantum Dots. *Phys. Rev. Lett.* **2001**, *87*, 157401.
(37) Fernee, M. J.; Sinito, C.; Louyer, Y.; Tamarat, P.; Lounis, B. The Ultimate Limit to the Emission Linewidth of Single Nanocrystals. *Nanotechnology* **2013**, *24*, 465103.
(38) Sangghaleh, F.; Bruhn, B.; Schmidt, T.; Linnros, J. Exciton Lifetime Measurements on Single Silicon Quantum Dots. *Nanotechnology* **2013**, *24*, 225204.
(39) Kovalev, D.; Heckler, H.; Ben-Chorin, M.; Polisski, G.; Schwartzkopff, M.; Koch, F. Breakdown of the k-Conservation Rule in Si Nanocrystals. *Phys. Rev. Lett.* **1998**, *81*, 2803−2806.
(40) Hybertsen, M. Absorption and Emission of Light in Nanoscale Silicon Structures. *Phys. Rev. Lett.* **1994**, *72*, 1514−1517.
(41) Sychugov, I.; Valenta, J.; Mitsuishi, K.; Linnros, J. Exciton Localization in Doped Si Nanocrystals from Single Dot Spectroscopy Studies. *Phys. Rev. B* **2012**, *86*, 075311.
(42) Lamb, H. On the Vibrations of an Elastic Sphere. *Proc. Math. Soc. London* **1882**, *13*, 189−212.
(43) Fujii, M.; Kanzawa, Y.; Hayashi, S.; Yamamoto, K. Raman Scattering from Acoustic Phonons Confined in Si Nanocrystals. *Phys. Rev. B* **1996**, *54*, R8373−R8376.
(44) Rufo, S.; Dutta, M.; Stroscio, M. A. Acoustic Modes in Free and Embedded Quantum Dots. *J. Appl. Phys.* **2003**, *93*, 2900−2905.
(45) Takagahara, T. Electron-Phonon Interactions in Semiconductor Nanocrystals. *J. Lumin.* **1996**, *70*, 129−143.
(46) Duval, E. Far-Infrared and Raman Vibrational Transitions of a Solid Sphere: Selection Rules. *Phys. Rev. B* **1992**, *46*, 5795−5797.
(47) Bruhn, B.; Valenta, J.; Sychugov, I.; Mitsuishi, K.; Linnros, J. Transition from Silicon Nanowires to Isolated Quantum Dots: Optical and Structural Evolution. *Phys. Rev. B* **2013**, *87*, 045404.
(48) Cui, J.; Beyler, A. P.; Marshall, L. F.; Chen, O.; Harris, D. K.; Wanger, D. D.; Brokmann, X.; Bawendi, M. G. Direct Probe of Spectral Inhomogeneity Reveals Synthetic Tunability of Single-Nanocrystal Spectral Linewidths. *Nat. Chem.* **2013**, *5*, 602−606.
(49) Empedocles, S. A.; Norris, D. J.; Bawendi, M. G. Photoluminescence Spectroscopy of Single CdSe Nanocrystallite Quantum Dots. *Phys. Rev. Lett.* **1996**, *77*, 3873−3876.
(50) Koberling, F.; Mews, A.; Basche, T. Single-Dot Spectroscopy of CdS Nanocrystals and CdS/HgS Heterostructures. *Phys. Rev. B* **1999**, *60*, 1921−1927.
(51) Perinetti, U.; Akopian, N.; Samsonenko, Y. B.; Bouravleuv, A. D.; Cirlin, G. E.; Zwiller, V. Sharp Emission from Single InAs Quantum Dots Grown on Vicinal GaAs Surfaces. *Appl. Phys. Lett.* **2009**, *94*, 163114.
(52) Pistol, M.-E.; Castrillo, P.; Hessman, D.; Anand, S.; Carlsson, N.; Seifert, W.; Samuelson, L. Band Filling in InP Dots: Single Dot Spectroscopy and Carrier Dynamics. *Solid-State Electron.* **1996**, *40*, 357−361.
(53) Gammon, D.; Snow, E. S.; Shanabrook, B. V.; Katzer, D. S.; Park, D. Fine Structure Splitting in the Optical Spectra of Single GaAs Quantum Dots. *Phys. Rev. Lett.* **1996**, *76*, 3005−3008.
(54) Kako, S.; Hoshino, K.; Iwamoto, S.; Ishida, S.; Arakawa, Y. Exciton and Biexciton Luminescence from Single Hexagonal GaN/AlN Self-Assembled Quantum Dots. *Appl. Phys. Lett.* **2004**, *85*, 64−66.
(55) Favero, I.; Cassabois, G.; Ferreira, R.; Darson, D.; Voisin, C.; Tignon, J.; Delalande, C.; Bastard, G.; Roussignol, Ph.; Gerard, J. M. Acoustic Phonon Sidebands in the Emission Line of Single InAs/GaAs Quantum Dots. *Phys. Rev. B* **2003**, *68*, 233301.
(56) Petterson, J.; Krauss, T. D. Fluorescence Spectroscopy of Single Lead Sulfide Quantum Dots. *Nano Lett.* **2006**, *6*, 510−514.